ACS APPLIED ENERGY MATERIALS

www.acsaem.org Article

ZnS-Nanoparticle-Coated Carbon Cloth as an Efficient Interlayer for High-Performance Li−S Batteries

Rui Liu,[#] Wei Tao,[#] Yingxia Du, Cuixia Wu, Huan Ye, Min Fan, Shuguang Chen, GuanHua Chen, Jianjun Mao,* Sen Xin,* and Fei-Fei Cao

Cite This: *ACS Appl. Energy Mater.* 2022, 5, 12408−12414 Read Online

ACCESS | Metrics & More | Article Recommendations | Supporting Information

ABSTRACT: Lithium−sulfur batteries are appealing electrochemical energy storage systems due to their potentially high energy output and low cost. At present, practical realization of Li−S batteries is hindered by unfavorable polysulfide shuttle during discharge−charge cycles, which causes capacity decay and sluggish kinetics of an electrode reaction. Metal sulfide catalysts were proposed to stabilize Li−S electrochemistry due to their ability to anchor polysulfides and facilitate their electrochemical conversion. In this work, zinc sulfide nanoparticles were synthesized and supported on a thin carbon cloth through a one-pot hydrothermal reaction. The catalyst-supported carbon cloth, with a low mass content of sulfides (2.18 wt %), could serve as a functional interlayer, absorbing the dissolved polysulfides and catalyzing the conversion reaction. As a result, the Li−S battery showed improved cycling performance with a high capacity retention of 93.5% after 100 cycles. This work demonstrates a rational strategy to realize high-performance Li−S batteries.

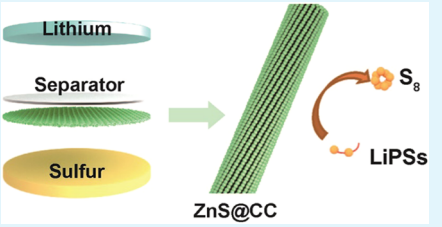

KEYWORDS: *lithium−sulfur batteries, zinc sulfide catalyst, functional interlayer, polysulfide adsorption and conversion*

1. INTRODUCTION

Lithium−sulfur batteries are regarded as one of the most promising choices for the next-generation electrochemical energy storage due to their high specific energy at the cell level (2567 Wh kg^{-1}).[1,2] Sulfur itself is an attractive cathode material owing to its high theoretical capacity (1675 mAh g^{-1}) *via* the two-electron redox reaction *versus* Li, nontoxic nature, and high resource abundance for large-scale manufacture.[3] Currently, several critical problems impede the practical use of Li−S batteries.[4] Sulfur naturally shows low bulk conductivity (5×10^{-30} S m^{-1} at room temperature)[5] and experiences drastic volume variation during Li uptake/release. Reducing the particle size of S to nanoscale is expected to facilitate charge transfer and alleviate volume variation during the electrochemical (de)lithiation of a S cathode, yet the Li−S system still involves other problems. It is known that the Li−S conversion reaction goes stepwisely, generating high-order lithium polysulfide (Li_2S_n, $4 \leq n \leq 8$) intermediates that are easily soluble in the organic electrolyte before they are further reduced to low-order polysulfides (Li_2S_m, $1 \leq m < 4$) or oxidized back to S.[6] The dissolved S species tend to shuttle to the Li anode, leading to an irreversible loss of active S from the cathode and the passivated Li anode surface. With the use of nano-S, the cathode may involve aggravated shuttle of lithium polysulfides (LiPSs) as the contact area between S and the electrolyte is enlarged. As a result, the Li−S battery usually shows inferior cycling performance and a low Coulombic efficiency.

Enormous efforts have been made to address the polysulfide shuttle issue, such as designing cathode host materials,[7,8] modifying functional separators,[9,10] building solid-state electrolytes,[11] and other approaches.[12] By introducing a functional carbon interlayer at the cathode side, the LIPS shuttle is expected to be inhibited, which accounts for improved storage performance of the Li−S battery. Various carbon materials, including carbon black,[13] microporous carbon,[14] mesoporous carbon,[15] and hierarchically porous carbon[16] were employed as an interlayer. During battery operation, carbon interlayers with a suitable porous structure (usually with mesopores and micropores) contribute to stronger physical adsorption of high-order LiPSs, while the high conductivity of carbon offsets the poor conductivity of S species and decreases the charge transfer resistance at cathode−electrolyte interface. However, nonpolar carbon usually shows a weak chemical interaction with polar LiPSs. To improve the LiPS−host binding and promote the redox reaction,[17,18] metal catalysts including metal oxides (e.g., VO_2[19] and Fe_3O_4[20]), metal carbides (e.g., TiC[21]), metal nitrides (e.g., TiN[17] and Co_4N[22]), and metal sulfides (e.g., WS_2,[23,24] TiS_2,[25] CoS_2,[26] and MoS_2[27]) were employed. The metal sulfides were extensively studied due to

Received: June 27, 2022
Accepted: September 13, 2022
Published: September 29, 2022

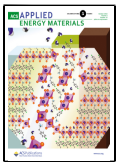

https://doi.org/10.1021/acsaem.2c02021
ACS Appl. Energy Mater. 2022, 5, 12408−12414

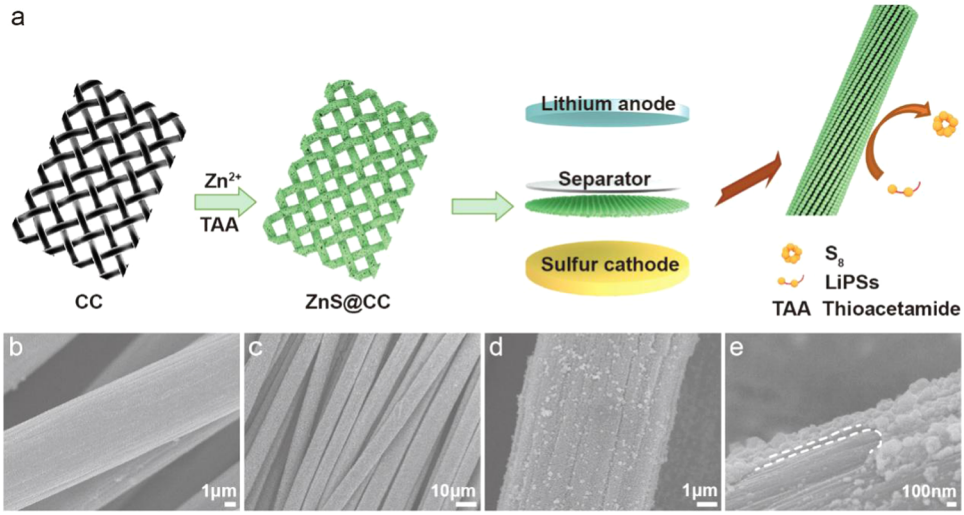

Figure 1. (a) Schematics of the fabrication process of ZnS@CC and the assembled cell model, (b) SEM image of treated CC, (c) and (d) low-magnification SEM images of ZnS@CC, and (e) high-magnification SEM image of ZnS@CC.

their high sulfiphilicity to LiPSs and low cost.[28] Zinc sulfide is a promising catalyst due to its significant cost advantage and ability to promote the LiPS redox kinetics.[29] According to Wang et al., zinc sulfide (ZnS) shows a high affinity to LiPSs, while also enables a low surface diffusion energy of LiPSs. However, ZnS shows a low bulk electronic conductivity (ca. 10^{-8} S cm^{-1}), and the introduction of an excessive amount of sulfide (e.g., ∼30 wt %) into the S cathode hinders charge transport and lowers the practical cathode capacity.

Here, we show that, instead of being directly applied into the cathode, coating a ZnS nanolayer (thickness: 50−70 nm) onto a conductive carbon cloth (ZnS@CC) yields a functional interlayer that effectively boosts the battery performance of the Li−S system. On the one hand, the conductive carbon cloth acts as a physical barrier to inhibit the shuttle effect of LiPSs while also provides paths for electron transport. Besides, the ZnS coating layer helps to chemically adsorb the LiPSs and catalyze the redox reaction. By incorporating the ZnS@CC interlayer, the sulfur/super P cathode shows an increased capacity of 30 mAh g^{-1} after 100 cycles at 0.1C (1C = 1675 mA g^{-1}) with an average capacity decay per cycle of 0.064%. Compared with the traditional carbon interlayer, ZnS@CC not only accelerates the kinetics of the cathode reaction but also opens a new direction for trapping LiPSs and promoting its conversion with less dosage of catalysts. Additionally, this one-pot hydrothermal strategy with low cost is feasible for large-scale preparation.

2. EXPERIMENTAL SECTION

2.1. Synthesis of ZnS@CC. Conductive carbon cloth (WOS 1002 PHYCHEMi Co. Ltd., China) was cut into slices (2 cm × 5 cm), thermally treated at 400 °C in air for 4 h, and rinsed with deionized water several times. The treated carbon cloth was then added to 60 mL of deionized water predissolved with 0.104 g off zinc nitrate hexahydrate ($Zn(NO_3)_2{\cdot}6H_2O$, Alfa Aesar, 98%) and 0.105 g of thioacetamide (C_2H_5NS, Acros Organics, 99%). The mixture was then transferred and sealed in a Teflon-lined stainless autoclave and heated at 180 °C for 12 h to yield the ZnS-decorated carbon cloth (ZnS@CC), which was then cut into discs with a diameter of 10 mm.

2.2. Preparation of the S Cathode. To prepare the S cathode, S (Sinopharm Chemical Reagent, 99.5%) was thoroughly mixed with Super P conductive carbon (Timical) and poly(vinylidene fluoride) (Arkema HSV900) binder at a weight ratio of 8:1:1, with the addition of N-methyl-2-pyrrolidinone (Sigma-Aldrich, 99.8%) to form a homogeneous slurry. The slurry was then pasted onto a carbon-coated Al foil (Hefei Kejing Corp., China) and dried in air at 60 °C for 12 h. Finally, the foil was cut into discs with a diameter of 10 mm and an average S mass loading of *ca.* 2.2 mg cm^{-2}.

2.3. Electrochemical Test. To test the electrochemical performance, the as-prepared S cathode was paired with a Li metal anode (Ganfengliye Corp., China) and was assembled into 2032-type coin cells in an Ar-filled glovebox (oxygen and water content: <0.1 ppm). A Celgard separator was used, and the prepared ZnS@CC disc was placed between the cathode and the separator. An electrolyte consisting of 1.0 M lithium bis(trifluoromethanesulphonyl)imide (LiTFSI) and a 1 wt % $LiNO_3$ additive in the solvent mixture of 1,3-dioxolane and 1,2-dimethoxymethane (1:1 by volume) was obtained from Nanjing Mojiesi Energy Technology Co. Ltd., and was used for assembling the cells at a fixed electrolyte/sulfur ratio of ca. 13 μL mg^{-1}. The galvanostatic charge−discharge tests were performed on a LAND CT-2001A battery tester within a voltage window of 1.7−2.8 V (vs Li^+/Li). The cyclic voltammetry (CV) profiles were collected on a Princeton ParSTAT MC (potential range: 1.5−3.0 V vs Li^+/Li; scan rate: 0.2 mV s^{-1}). Electrochemical impedance spectroscopy (EIS) was performed on a Princeton ParSTAT MC (frequency range: 0.1−100 MHz).

Other experimental details, including Material Characterization, Absorption Test, and Computational Method, are given in the Supporting Information.

3. RESULTS AND DISCUSSION

Figure 1a shows the preparation of ZnS@CC and the schematic of the assembled Li−S cell. We synthesized ZnS nanoparticles by the method of the one-pot hydrothermal reaction. The ZnS nanoparticles attached to the carbon cloth were well dispersed. During the solvothermal treatment, ZnS nanoparticles were formed on carbon cloth (CC). The electrons could be effectively transmitted through the carbon fiber, and the LiPSs formed in the cathode reached near the ZnS nanoparticles on the surface of the interlayer ZnS@CC in the process of diffusion. The chemical adsorption was enhanced after the combination of ZnS and LiPSs, and the active materials could be firmly fixed on the cathode side because of the high conversion of LiPSs. This effectively inhibited the loss of LIPSs diffused to the lithium metal anode. Compared with bare CC owning a smooth surface (Figure 1b), scanning electron microscopy (SEM) images of ZnS@CC

https://doi.org/10.1021/acsaem.2c02021
ACS Appl. Energy Mater. 2022, 5, 12408−12414

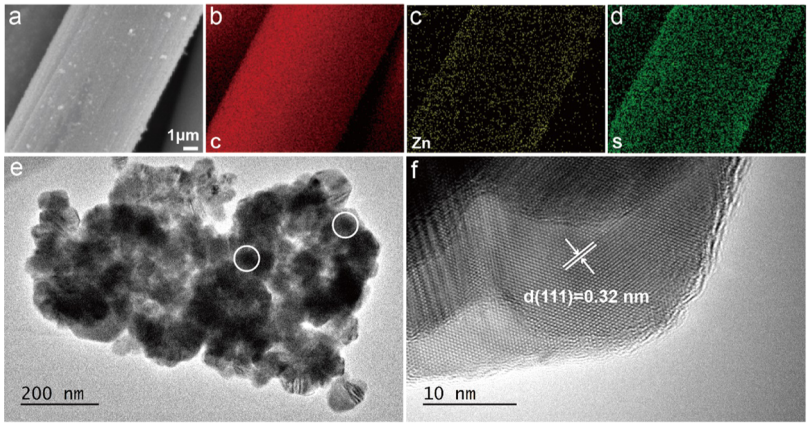

Figure 2. (a) SEM image of ZnS@CC, corresponding to the elemental mapping of (b) C, (c) Zn, and (d) S. (e) TEM image of ZnS nanoparticles and (f) HRTEM image of ZnS nanoparticles.

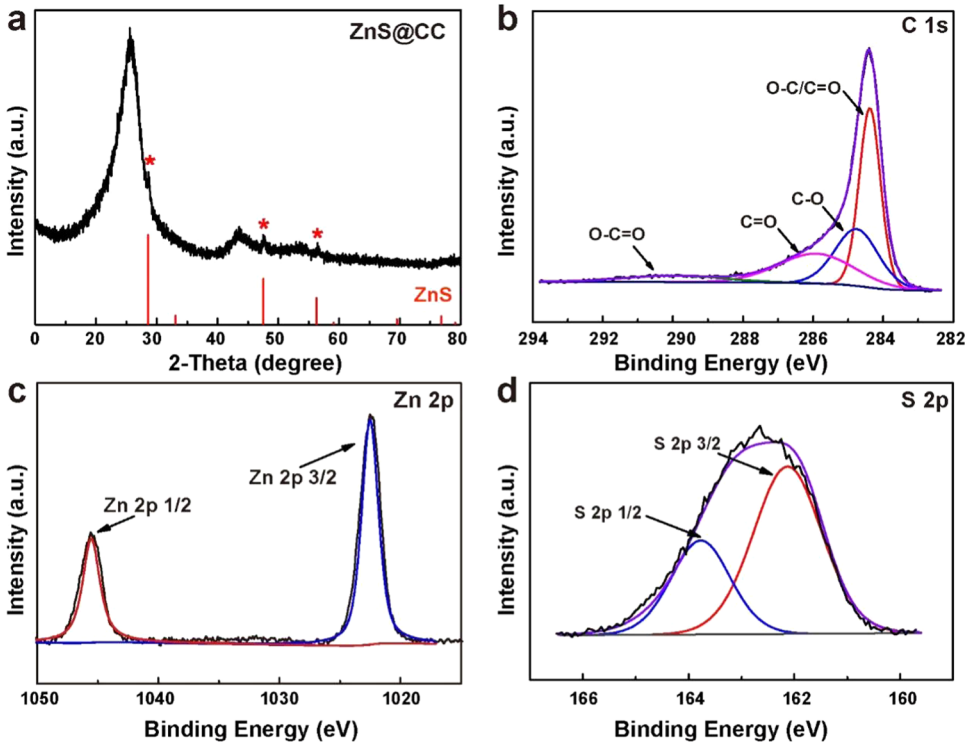

Figure 3. (a) XRD pattern of ZnS@CC. High-resolution (b) C 1s, (c) Zn 2p, and (d) S 2p XPS spectra of ZnS@CC.

show that CC is evenly coated with ZnS nanoparticles with a thickness of 50−70 nm (Figure 1c−e). In addition, a typical transmission electron microscopy (TEM) image of the carbon fibers coated with ZnS is provided in Figure 2e and shows that the ZnS nanoparticles possess an average size of ∼30 nm. Elemental mappings of ZnS@CC further confirm the uniform distribution of ZnS nanoparticles on the CC surface (Figure 2a−d).

In the X-ray diffraction (XRD) pattern of ZnS@CC (Figure 3a), typical peaks of ZnS are observed, among which the peaks at 28.5, 47.6, and 56.3° correspond to the (111), (220), and (311) planes, respectively (JCPD no. 05−0566). In the high-resolution TEM (HRTEM) image of ZnS@CC (Figure 2f), an interplanar spacing of 0.32 nm is observed and corresponds to the (111) plane of ZnS.[30] Two broad peaks at around 26 and 43° are assigned to amorphous carbon and partial graphitic carbon derived from the carbon cloth. The above phase analysis indicates that the product obtained is the compound of carbon cloth and ZnS. In addition, there is no obvious impurity peak in the figure, indicating that there is no excess impurity in the synthesized materials. However, the peak corresponding to ZnS is not strong because the ZnS layer coated on the surface of the carbon cloth is thin and the mass ratio is very low. The content of ZnS in ZnS@CC is characterized by thermogravimetry analyses (TGA). As shown in Figure S1, the weight loss of ZnS happens during the heating process in air due to the combustion of carbon fibers with air and the conversion of ZnS into zinc oxide (ZnO). Therefore, the mass ratio of ZnS is calculated to be 2.18% based on the amount of ZnO (1.82 wt %) in the final residues.[31]

The composition of ZnS@CC was further investigated by X-ray photoelectron spectroscopy (XPS). Figure S2 shows the full survey XPS spectrum of ZnS@CC, and the peaks at 162.7,

https://doi.org/10.1021/acsaem.2c02021
ACS Appl. Energy Mater. 2022, 5, 12408−12414

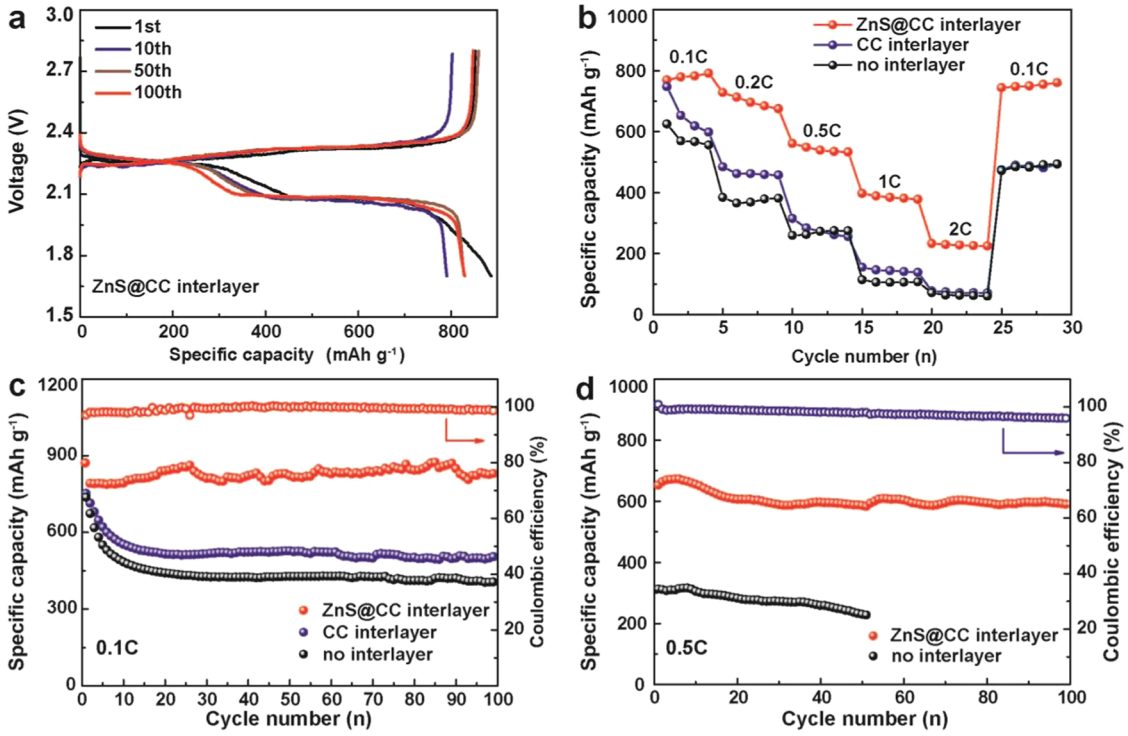

Figure 4. (a) Discharge−charge profiles of the Li−S cell with a ZnS@CC interlayer after different cycles at 0.1C. (b) Rate performance of the Li−S cell with different interlayers at different current densities. (c) Cycling performance of the Li−S cell with different interlayers at 0.1C. (d) Cycling performance of the Li−S cell with different interlayers at 0.5C.

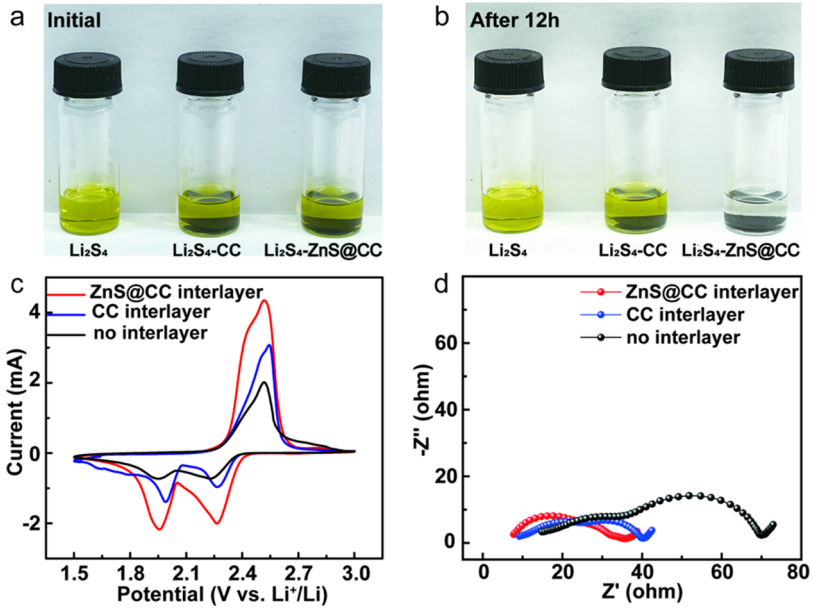

Figure 5. Visualized adsorption of Li_2S_4 on ZnS@CC and CC with a control experiment: (a) initial and (b) after 12 h. (c) CV profiles of the Li−S cell with different interlayers. (d) EIS spectra of the Li−S cell with different interlayers after activation of three cell cycles at 0.1C.

284.4, 531.8, and 1022.5 eV correspond to S 2p, C 1s, O 1s, and Zn 2p, respectively. According to the C 1s spectrum (Figure 3b), the four peaks at 284.3, 284.8, 285.9, and 290.0 eV correspond to C−C/C═C, C−O, C═O, and O−C═O, respectively.[32] In Figure 3c, two peaks of the spin orbits of Zn $2p^{3/2}$ and Zn $2p^{1/2}$ appear at 1022.5 and 1045.6 eV, respectively, indicating the presence of Zn 2p.[29] Referring to the enlarged S 2p spectrum of ZnS@CC (Figure 3d), two peaks at 162.1 and 163.8 eV correspond to the S $2p^{3/2}$ and S $2p^{1/2}$ peaks of the S^{2-} anion.[33] The XPS findings agree with the above phase analysis.

Figure 4a shows the galvanostatic discharge/charge profiles of the Li−S cell at 0.1C (1C = 1675 mA g^{-1}). The cell exhibits two typical discharge plateaus that are ascribed to the two-step lithiation reaction of S. As we can see, with the increase in the cycling number, the capacity did not decay but got a certain increase because active materials in the cathode are activated after cycling with the introduction of the ZnS@CC interlayer.

https://doi.org/10.1021/acsaem.2c02021
ACS Appl. Energy Mater. 2022, 5, 12408−12414

Figure 4c compares the cycling performance of Li−S cells assembled with different interlayers. The one with ZnS@CC shows an initial discharge capacity of 887 mAh g^{-1} and a reversible discharge capacity of 830 mAh g^{-1} after 100 cycles, which corresponds to a low-capacity decay of 0.064% per cycle. The performance data are superior to those obtained from the Li−S cells with a CC interlayer (502 mAh g^{-1} after 100 cycles) or no interlayer (427 mAh g^{-1} after 100 cycles) in the control experiments, and other interlayer-loaded Li−S cells provided in Table S1. Therefore, it is apparent that the introduction of the ZnS@CC interlayer significantly improves the capacity output and cycling performance of the Li−S cell. Figure 4b evaluates the rate capabilities of the Li−S cells assembled with ZnS@CC, CC, and no interlayer at various C rates (0.1, 0.2, 0.5, 1, 2, and back to 0.1C). The capacity of these three cells decreases with increasing rate, yet the rate capability of the Li−S cell with the ZnS@CC interlayer is significantly higher than the control cells. At a high rate of 2C, the cell with the ZnS@CC interlayer is still able to deliver a reversible capacity of 233 mAh g^{-1}, while the two control cells barely deliver ca. 50 mAh g^{-1}. Upon reducing the C rate back to 0.1C, the cell with the ZnS@CC interlayer can restore a reversible capacity of 744 mAh g^{-1}. According to Figure 4d (rate: 0.5C), the cell with the ZnS@CC interlayer shows a reversible capacity of 590 mAh g^{-1} after 100 cycles and a capacity decline of 0.096% per cycle. In the control experiment, a Li−S cell without an interlayer displays a significantly lower initial discharge capacity of 313 mAh g^{-1}.

The improved cell performance is attributed to the potent affinity of the ZnS@CC interlayer on LiPSs and its catalytic role in the conversion reaction of LiPSs. The materials with catalytic properties can promote the kinetic conversion of LiPSs, and their chemical adsorption on LiPSs will be conducive to the next catalytic conversion of LiPSs. Therefore, we further verify the interfacial interaction between the ZnS@CC interlayer with LiPSs, and the adsorption of Li_2S_4 (typical LiPSs) on ZnS@CC and CC is performed. As shown in Figure 5a,b, after adding ZnS@CC in 10 mmol/L Li_2S_4 solutions for 12 h, the color of the Li_2S_4 solution (yellow) obviously faded, while the color changed less after the CC was immersed in Li_2S_4 at the same conditions, revealing the strong adsorption ability of ZnS. In addition, Figure S3 compares the color of Celgard separators in Li−S batteries with a sulfur cathode after 100 cycles at 0.5C using a ZnS@CC interlayer or not. It is obvious that the color of the separator with the ZnS@CC interlayer hardly changes, but the separator without the ZnS@CC interlayer is obviously yellow. These different phenomena indicate the strong chemical adsorption of the ZnS@CC interlayer; this provides a favorable condition for ZnS@CC to catalyze the transformation reaction of LIPSs. Figure 5c collects the CV profiles of the Li−S cells with the ZnS@CC interlayer, the CC interlayer, and no interlayer. Two typical reduction peaks that correspond to electrochemical conversion from cyclo-S_8 to high-order LiPSs (Li_2S_n, $4 \le n \le 8$) and from high-order LiPSs to insoluble low-order LiPSs (Li_2S_n, $1 \le n < 4$) are observed for the three cells. However, the cell with the ZnS@CC interlayer shows notably higher redox current, indicating improved reaction kinetics of the S cathode.[34]

After activation of three cell cycles at 0.1C, the EIS measurement is further performed to illustrate the influence of the ZnS@CC interlayer on the electrochemical performance of Li−S batteries. It is found that three Nyquist plots consist of a high-frequency semicircle and a low-frequency slope line, which are associated with the charge transfer resistance and the Li^+ diffusion resistance separately.[35−37] Apparently, as we can see in Figure 5d, the semicircle diameters using the ZnS@CC interlayer are smaller than those using the CC interlayer or with no interlayer, proving the significantly enhanced electrochemical kinetics of the sulfur cathode with the ZnS@CC interlayer. Using ZnS@CC as a barrier layer can greatly reduce the charge transfer impedance in the Li−S battery, which is another strong proof of the improvement of the electrochemical dynamics inside the battery.

Density functional theory (DFT) calculations[38,39] were carried out to study the adsorption energies of typical LiPS species (e.g., Li_2S_4, according to Xu et al.[40]). As shown in Figure 6a, the adsorption energies of Li_2S_4 on the graphite and

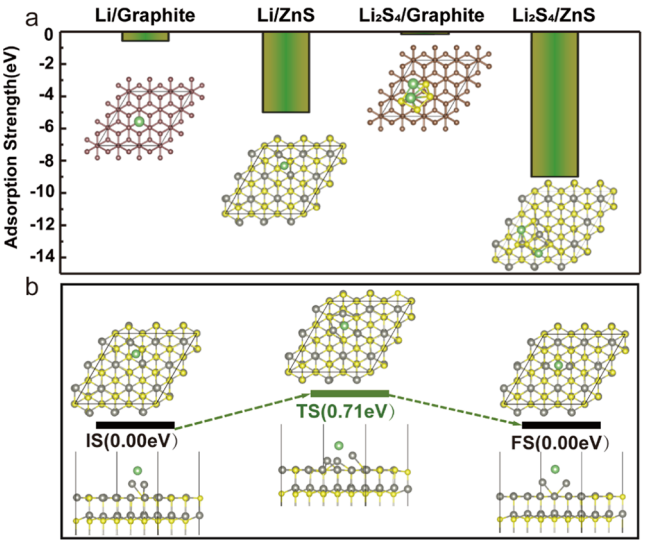

Figure 6. (a) Visualized adsorption of Li_2S_4 on ZnS@CC and CC with a control experiment: The adsorption energies for Li and Li_2S_4 on graphite(001) and ZnS(001); most stable adsorption configurations are given. C, Li, S, and Zn are shown as brown, green, yellow, and gray spheres, respectively. (b) Schematic potential profiles for Li diffusion on the ZnS surface. The initial state, transition state, and final state are denoted by "IS", "TS", and "FS", respectively.

ZnS are 0.15 and 9.18 eV, respectively, confirming that the ZnS@CC interlayer has a strong ability to adsorb polysulfides. The Li^+ diffusion pathways on the (001) facets of ZnS (Figure 6b) and graphite (Figure S4) were also calculated and compared. The energy barrier for Li^+ diffusion along the ZnS (001) facet is 0.71 eV, which is significantly lower than that along the graphite (001) facet (5.70 eV). The above results indicate that the introduction of the ZnS@CC interlayer not only inhibits the shuttle of LiPSs but also facilitates Li^+ transfer in the cell, which could be the reason for the improved cathode kinetics.

4. CONCLUSIONS

In conclusion, we have demonstrated a multifunctional ZnS@CC interlayer of Li−S batteries. The preparation method is feasible to operate, and the mass ratio of ZnS is greatly reduced by coating a nanoparticle catalyst on the conductive skeleton surface. ZnS nanoparticles (2.18 wt %) play a critical role in adsorbing the migrating LiPSs and accelerating the kinetics redox reactions of LiPS conversion, while carbon cloth affords enhanced electrical conductivity. Moreover, our DFT calculations proved that the high adsorption energies of polysulfide

https://doi.org/10.1021/acsaem.2c02021
ACS Appl. Energy Mater. 2022, 5, 12408−12414

and the low Li ion diffusion barrier on ZnS restricted the shuttle of polysulfides and promoted the polysulfide redox reaction. The sulfur cathode with the ZnS@CC interlayer exhibits an enhanced capacity retention of 93.5% after 100 cycles at 0.1C. The rational designing strategy of the ZnS@CC interlayer provides a new way to decrease the number of activation catalysts for practical application in the future.

■ ASSOCIATED CONTENT

Supporting Information

The Supporting Information is available free of charge at https://pubs.acs.org/doi/10.1021/acsaem.2c02021.

TGA of ZnS@CC, full survey XPS spectrum, optical contrast diagram of the Celgard separator after 100 cycles, and schematic potential profiles for Li^+ diffusion on the graphite surface (PDF)

■ AUTHOR INFORMATION

Corresponding Authors

Jianjun Mao − *Department of Chemistry, The University of Hong Kong, Hong Kong 999077, P. R. China; Hong Kong Quantum AI Lab Limited, Hong Kong 999077, P. R. China;* orcid.org/0000-0003-2265-9685; Email: jjmao@connect.hku.hk

Sen Xin − *CAS Key Laboratory of Molecular Nanostructure and Nanotechnology, CAS /Research/Education Center for Excellence in Molecular Sciences, Beijing National Laboratory for Molecular Sciences (BNLMS), Institute of Chemistry, Chinese Academy of Sciences (CAS), Beijing 100190, P. R. China;* orcid.org/0000-0002-0546-0626; Email: xinsen08@iccas.ac.cn

Authors

Rui Liu − *Department of Chemistry, College of Science, Huazhong Agricultural University, Wuhan 430070, P. R. China*

Wei Tao − *Department of Chemistry, College of Science, Huazhong Agricultural University, Wuhan 430070, P. R. China*

Yingxia Du − *Department of Chemistry, College of Science, Huazhong Agricultural University, Wuhan 430070, P. R. China; College of Resources and Environment, Huazhong Agricultural University, Wuhan 430070, P. R. China*

Cuixia Wu − *Department of Chemistry, College of Science, Huazhong Agricultural University, Wuhan 430070, P. R. China*

Huan Ye − *Department of Chemistry, College of Science, Huazhong Agricultural University, Wuhan 430070, P. R. China;* orcid.org/0000-0002-1074-528X

Min Fan − *CAS Key Laboratory of Molecular Nanostructure and Nanotechnology, CAS /Research/Education Center for Excellence in Molecular Sciences, Beijing National Laboratory for Molecular Sciences (BNLMS), Institute of Chemistry, Chinese Academy of Sciences (CAS), Beijing 100190, P. R. China*

Shuguang Chen − *Department of Chemistry, The University of Hong Kong, Hong Kong 999077, P. R. China; Hong Kong Quantum AI Lab Limited, Hong Kong 999077, P. R. China*

GuanHua Chen − *Department of Chemistry, The University of Hong Kong, Hong Kong 999077, P. R. China; Hong Kong Quantum AI Lab Limited, Hong Kong 999077, P. R. China;* orcid.org/0000-0001-5015-0902

Fei-Fei Cao − *Department of Chemistry, College of Science, Huazhong Agricultural University, Wuhan 430070, P. R. China;* orcid.org/0000-0002-4290-2032

Complete contact information is available at: https://pubs.acs.org/10.1021/acsaem.2c02021

Author Contributions

#R.L. and W.T. contributed equally to this work.

Notes

The authors declare no competing financial interest.

■ ACKNOWLEDGMENTS

This work was supported by the National Key R&D Program of China (Grant No 2019YFA0705703), the National Natural Science Foundation of China (Nos. 21773078, 21975266, 52172252), the Natural Science Foundation of Hubei Province (No. 2019CFA046), and the Fundamental Research Funds for the Central Universities of China (Nos. 2662020LXPY006, 20230614). J.M., S.C., and G.C. acknowledge the support from Hong Kong Quantum AI Lab Ltd.

■ REFERENCES

(1) Lei, T. Y.; Chen, W.; Huang, J. W.; Yan, C. Y.; Sun, H. X.; Wang, C.; Zhang, W. L.; Li, Y. R.; Xiong, J. Multi- Functional Layered WS_2 Nanosheets for Enhancing the Performance of Lithium-Sulfur Batteries. *Adv. Energy Mater.* **2017**, *7*, No. 1601843.

(2) He, J. R.; Luo, L.; Chen, Y. F.; Manthiram, A. Yolk-Shelled C@Fe_3O_4 Nanoboxes as Efficient Sulfur Hosts for High-Performance Lithium-Sulfur Batteries. *Adv. Mater.* **2017**, *29*, No. 1702707.

(3) Dai, C. L.; Lim, J. M.; Wang, M. Q.; Hu, L. Y.; Chen, Y. M.; Chen, Z. Y.; Chen, H.; Bao, S. J.; Shen, B. L.; Li, Y.; et al. Honeycomb-Like Spherical Cathode Host Constructed from Hollow Metallic and Polar Co_9S_8 Tubules for Advanced Lithium-Sulfur Batteries. *Adv. Funct. Mater.* **2018**, *28*, No. 1704443.

(4) Wu, X.; Liu, N. N.; Wang, M. X.; Qiu, Y.; Guan, B.; Tian, D.; Guo, Z. K.; Fan, L. S.; Zhang, N. Q. A Class of Catalysts of BiO_X (X = Cl, Br, I) for Anchoring Polysulfides and Accelerating Redox Reaction in Lithium Sulfur Batteries. *ACS Nano* **2019**, *13*, 13109−13115.

(5) Hu, L. Y.; Dai, C. L.; Liu, H.; Li, Y.; Shen, B. L.; Chen, Y. M.; Bao, S. J.; Xu, M. W. Double-Shelled NiO-$NiCo_2O_4$ Heterostructure@Carbon Hollow Nanocages as an Efficient Sulfur Host for Advanced Lithium-Sulfur Batteries. *Adv. Energy Mater.* **2018**, *8*, No. 1800709.

(6) Li, L.; Chen, L.; Mukherjee, S.; Gao, J.; Sun, H.; Liu, Z. B.; Ma, X. L.; Gupta, T.; Singh, C. V.; Ren, W. C.; et al. Phosphorene as a Polysulfide Immobilizer and Catalyst in High-Performance Lithium-Sulfur Batteries. *Adv. Mater.* **2017**, *29*, No. 1602734.

(7) Li, Z.; Wu, H. B.; Lou, X. W. Rational Designs and Engineering of Hollow Micro-/Nanostructures as Sulfur Hosts for Advanced Lithium-Sulfur Batteries. *Energy Environ. Sci.* **2016**, *9*, 3061−3070.

(8) Sun, Y. M.; Liu, N. A.; Cui, Y. Promises and Challenges of Nanomaterials for Lithium-Based Rechargeable Batteries. *Nat. Energy* **2016**, *1*, No. 16071.

(9) Bai, S.; Liu, X.; Zhu, K.; Wu, S.; Zhou, H. Metal-organic Framework-Based Separator for Lithium-Sulfur Batteries. *Nat. Energy* **2016**, *1*, No. 16094.

(10) Du, Z.; Guo, C.; Wang, L.; Hu, A.; Jin, S.; Zhang, T.; Jin, H.; Qi, Z.; Xin, S.; Kong, X.; et al. Atom-Thick Interlayer Made of CVD-Grown Graphene Film on Separator for Advanced Lithium-Sulfur Batteries. *ACS Appl. Mater. Interfaces* **2017**, *9*, 43696−43703.

(11) Wang, W. P.; Zhang, J.; Chou, J.; Yin, Y. X.; You, Y.; Xin, S.; Guo, Y. G. Solidifying Cathode−Electrolyte Interface for Lithium−Sulfur Batteries. *Adv. Energy Mater.* **2020**, *11*, No. 2000791.

(12) Shao, Q.; Wu, Z.-S.; Chen, J. Two-Dimensional Materials for Advanced Li-S batteries. *Energy Storage Mater.* **2019**, *22*, 284−310.

(13) Ye, Y.; Wang, L.; Guan, L.; Wu, F.; Qian, J.; Zhao, T.; Zhang, X.; Xing, Y.; Shi, J.; Li, L.; Chen, R. A Modularly-Assembled Interlayer to Entrap Polysulfides and Protect Lithium Metal Anode for High Areal Capacity Lithium−Sulfur Batteries. *Energy Storage Mater.* **2017**, *9*, 126−133.
(14) Yang, J.; Chen, F.; Li, C.; Bai, T.; Long, B.; Zhou, X. A Free-Standing Sulfur-Doped Microporous Carbon Interlayer Derived from Luffa Sponge for High Performance Lithium−Sulfur Batteries. *J. Mater. Chem. A* **2016**, *4*, 14324−14333.
(15) Zhao, T.; Ye, Y.; Peng, X.; Divitini, G.; Kim, H.-K.; Lao, C.-Y.; Coxon, P. R.; Xi, K.; Liu, Y.; Ducati, C.; et al. Advanced Lithium−Sulfur Batteries Enabled by a Bio-Inspired Polysulfide Adsorptive Brush. *Adv. Funct. Mater.* **2016**, *26*, 8418−8426.
(16) Wang, J.; Jiang, K.; Shen, B.; Zhen, M. Synergetic Effect of Nitrogen/Sulfur Dual-Doped Hierarchically Porous Carbon Networks for Li−S Batteries. *ACS Sustainable Chem. Eng.* **2020**, *8*, 749−758.
(17) Jeong, T. G.; Choi, D. S.; Song, H.; Choi, J.; Park, S. A.; Oh, S. H.; Kim, H.; Jung, Y.; Kim, Y. T. Heterogeneous Catalysis for Lithium-Sulfur Batteries: Enhanced Rate Performance by Promoting Polysulfide Fragmentations. *ACS Energy Lett.* **2017**, *2*, 327−333.
(18) Li, G.; Wang, X. L.; Seo, M. H.; Li, M.; Ma, L.; Yuan, Y. F.; Wu, T. P.; Yu, A. P.; Wang, S.; Lu, J.; Chen, Z. Chemisorption of Polysulfides Through Redox Reactions with Organic Molecules for Lithium-Sulfur Batteries. *Nat. Commun.* **2018**, *9*, No. 705.
(19) Song, Y. Z.; Zhao, W.; Kong, L.; Zhang, L.; Zhu, X. Y.; Shao, Y. L.; Ding, F.; Zhang, Q.; Sun, J. Y.; Liu, Z. F. Synchronous Immobilization and Conversion of Polysulfides on a VO_2-VN Binary Host Targeting High Sulfur Load Li-S Batteries. *Energy Environ. Sci.* **2018**, *11*, 2620−2630.
(20) Lu, K.; Zhang, H.; Gao, S.; Ma, H.; Chen, J.; Cheng, Y. Manipulating Polysulfide Conversion with Strongly Coupled Fe_3O_4 and Nitrogen Doped Carbon for Stable and High Capacity Lithium-Sulfur Batteries. *Adv. Funct. Mater.* **2019**, *29*, No. 1807309.
(21) Zhou, F.; Li, Z.; Luo, X.; Wu, T.; Jiang, B.; Lu, L. L.; Yao, H. B.; Antonietti, M.; Yu, S. H. Low Cost Metal Carbide Nanocrystals as Binding and Electrocatalytic Sites for High Performance Li-S Batteries. *Nano Lett.* **2018**, *18*, 1035−1043.
(22) Xiao, K.; Wang, J.; Chen, Z.; Qian, Y.; Liu, Z.; Zhang, L.; Chen, X.; Liu, J.; Fan, X.; Shen, Z. X. Improving Polysulfides Adsorption and Redox Kinetics by the Co_4N Nanoparticle/N-Doped Carbon Composites for Lithium-Sulfur Batteries. *Small* **2019**, *15*, No. 1901454.
(23) Park, J.; Yu, B. C.; Park, J. S.; Choi, J. W.; Kim, C.; Sung, Y. E.; Goodenough, J. B. Tungsten Disulfide Catalysts Supported on a Carbon Cloth Interlayer for High Performance Li-S Battery. *Adv. Energy Mater.* **2017**, *7*, No. 1602567.
(24) Babu, G.; Masurkar, N.; Al Salem, H.; Arave, L. M. R. Transition Metal Dichalcogenide Atomic Layers for Lithium Polysulfides Electrocatalysis. *J. Am. Chem. Soc.* **2017**, *139*, 171−178.
(25) Zhou, G. M.; Tian, H. Z.; Jin, Y.; Tao, X. Y.; Liu, B. F.; Zhang, R. F.; Seh, Z. W.; Zhuo, D.; Liu, Y. Y.; Sun, J.; et al. Catalytic Oxidation of Li_2S on the Surface of Metal Sulfides for Li-S Batteries. *Proc. Natl. Acad. Sci. U.S.A.* **2017**, *114*, 840−845.
(26) Liu, D. H.; Zhang, C.; Zhou, G. M.; Lv, W.; Ling, G. W.; Zhi, L. J.; Yang, Q. H. Catalytic Effects in Lithium-Sulfur Batteries: Promoted Sulfur Transformation and Reduced Shuttle Effect. *Adv. Sci.* **2018**, *5*, No. 1700270.
(27) Lin, H.; Yang, L.; Jiang, X.; Li, G.; Zhang, T.; Yao, Q.; Zheng, G. W.; Lee, J. Y. Electrocatalysis of Polysulfide Conversion by Sulfur-Deficient MoS_2 Nanoflakes for Lithium-Sulfur Batteries. *Energy Environ. Sci.* **2017**, *10*, 1476−1486.
(28) Razaq, R.; Sun, D.; Wang, J.; Xin, Y.; Abbas, G.; Zhang, J. H.; Li, Q.; Huang, T. Z.; Zhang, Z. L.; Huang, Y. H. Ultrahigh Sulfur Loading in ZnS_{1-x}/rGO through in Situ Oxidation-Refilling Route for High-Performance Li-S Batteries. *J. Power Sources.* **2019**, *414*, 453−459.
(29) Xu, J.; Zhang, W. X.; Fan, H. B.; Cheng, F. L.; Su, D. W.; Wang, G. X. Promoting Lithium Polysulfide/Sulfide Redox Kinetics by the Catalyzing of Zinc Sulfide for High Performance Lithium-Sulfur Battery. *Nano Energy* **2018**, *51*, 73−82.
(30) Xu, Z. C.; Zhang, Z. Q.; Li, M. Y.; Yin, H. L.; Lin, H. T.; Zhou, J.; Zhuo, S. P. Three-Dimensional ZnS/Reduced Graphene Oxide/Polypyrrole Composite for High-Performance Supercapacitors and Lithium-Ion Battery Electrode Material. *J. Solid State Electrochem.* **2019**, *23*, 3419−3428.
(31) Jing, M. J.; Chen, Z. G.; Li, Z.; Li, F. Y.; Chen, M. J.; Zhou, M. J.; He, B. H.; Chen, L.; Hou, Z. H.; Chen, X. B. Facile Synthesis of ZnS/N, S Co-doped Carbon Composite from Zinc Metal Complex for High-Performance Sodium-Ion Batteries. *ACS Appl. Mater. Interfaces* **2018**, *10*, 704−712.
(32) Sun, Q.; Xi, B. J.; Li, J. Y.; Mao, H. Z.; Ma, X. J.; Liang, J. W.; Feng, J. K.; Xiong, S. L. Nitrogen-Doped Graphene-Supported Mixed Transition-Metal Oxide Porous Particles to Confine Polysulfides for Lithium-Sulfur Batteries. *Adv. Energy Mater.* **2018**, *8*, No. 1800595.
(33) Zhao, W.; Zheng, Y. W.; Cui, L.; Jia, D. D.; Wei, D.; Zheng, R. K.; Barrow, C.; Yang, W. R.; Liu, J. Q. MOF derived Ni-Co-S Nanosheets on Electrochemically Activated Carbon Cloth via an Etching/Ion Exchange Method for Wearable Hybrid Supercapacitors. *Chem. Eng. J.* **2019**, *371*, 461−469.
(34) Al Salem, H.; Babu, G.; Rao, C. V.; Arava, L. M. R. Electrocatalytic Polysulfide Traps for Controlling Redox Shuttle Process of Li-S Batteries. *J. Am. Chem. Soc.* **2015**, *137*, 11542−11545.
(35) Huang, X.; Yang, C.; You, Y. Polycrystalline Prussian White Aggregates as a High-Rate and Long-Life Cathode for High-Temperature Sodium-Ion Batteries. *ACS Appl. Energy Mater.* **2022**, *5*, 8123−8131.
(36) Zhang, S.; Qiu, L.; Zheng, Y.; Shi, Q.; Zhou, T.; Sencadas, V.; Xu, Y.; Zhang, S.; Zhang, L.; Zhang, C.; et al. Rational Design of Core-Shell ZnTe@N-Doped Carbon Nanowires for High Gravimetric and Volumetric Alkali Metal Ion Storage. *Adv. Funct. Mater.* **2021**, *31*, No. 2006425.
(37) Lin, Y.; Yang, C.; You, Y. Improving Sodium Storage Performance of Hard Carbon Anodes in Cyclic Ether Electrolytes by an Anion Receptor Additive. *J. Electrochem. Soc.* **2022**, *169*, No. 020561.
(38) Grimme, S.; Antony, J.; Ehrlich, S.; Krieg, H. A Consistent and Accurate Ab Initio Parametrization of Density Functional Dispersion Correction (DFT-D) for the 94 Elements H-Pu. *J. Chem. Phys.* **2010**, *132*, No. 154104.
(39) Henkelman, G.; Uberuaga, B. P.; Jonsson, H. A Climbing Image Nudged Elastic Band Method for Finding Saddle Points and Minimum Energy Paths. *J. Chem. Phys.* **2000**, *113*, 9901−9904.
(40) Xu, J.; Zhang, W.; Fan, H.; Cheng, F.; Su, D.; Wang, G. Promoting Lithium Polysulfide/Sulfide Redox Kinetics by the Catalyzing of Zinc Sulfide for High Performance Lithium-Sulfur Battery. *Nano Energy* **2018**, *51*, 73−82.

https://doi.org/10.1021/acsaem.2c02021
ACS Appl. Energy Mater. 2022, 5, 12408−12414